GEM - International Journal on Geomathematics (2019) 10:23
https://doi.org/10.1007/s13137-019-0136-4

ORIGINAL PAPER

Nonlocal multicontinuum (NLMC) upscaling of mixed dimensional coupled flow problem for embedded and discrete fracture models

Maria Vasilyeva[1,2] · Eric T. Chung[3] · Wing Tat Leung[4] · Valentin Alekseev[5]

Received: 4 May 2018 / Accepted: 12 September 2019 / Published online: 20 September 2019

Abstract
In this work, we present an upscaled model for mixed dimensional coupled flow problem in fractured porous media. We consider both embedded and discrete fracture models (EFM and DFM) as fine scale models which contain coupled system of equations. For fine grid discretization, we use a conservative finite-volume approximation. We construct an upscaled model using the non-local multicontinuum (NLMC) method for the coupled system. The proposed upscaled model is based on a set of simplified multiscale basis functions for the auxiliary space and a constraint energy minimization principle for the construction of multiscale basis functions. Using the constructed NLMC-multiscale basis functions, we obtain an accurate coarse grid upscaled model. We present numerical results for both fine-grid models and upscaled coarse-grid models using our NLMC method. We consider model problems with (1) discrete fracture fine grid model with low and high permeable fractures; (2) embedded fine grid model for two types of geometries with differnet fracture networks and (3) embedded fracture fine grid model with heterogeneous permeability. The simulations using the upscaled model provide very accurate solutions with significant reduction in the dimension of the problem.

Keywords Fractured porous media · Single phase flow · Mixed dimensional problem · Mulitscale method · Upscaling · Nonlocal multicontinua method

Mathematics Subject Classification 65M08 · 65M60

1 Introduction

Mathematical simulation of the flow processes in fractured porous media plays an important role in reservoir simulation, nuclear waste disposal, CO_2 sequestration, unconventional gas production and geothermal energy production. Fracture networks

Extended author information available on the last page of the article

usually have complex geometries, multiple scales and very small thickness compared to typical reservoir sizes. Due to high permeability, fractures have a significant impact on the flow processes. A common approach to model fracture media is to consider the discrete fractures as lower-dimensional objects (Martin et al. 2005; D'Angelo and Scotti 2012; Formaggia et al. 2014; D'angelo and Quarteroni 2008; Schwenck et al. 2015). This results in a coupled mixed dimensional mathematical models, where we have d-dimensional equation for flow in porous matrix and $(d-1)$-dimensional equation for fracture networks. The cross-flow equilibrium between the flow in fracture and matrix is described by some specific transfer terms.

Various numerical approaches to model fractured porous media have been developed and can be classified by the types of meshing techniques used for simulations. One approach, called discrete fracture model (DFM) is associated with the conforming discretization or explicit meshing of the fracture geometry. In DFM, we consider flow processes in both the matrix and the fracture media, where the fractures are located at the interfaces between matrix cells (Hoteit and Firoozabadi 2008; Karimi-Fard et al. 2003; Karimi-Fard and Firoozabadi 2001; Garipov et al. 2016). This requires a conforming meshing of the fractures, which can lead to large computational demands since a large number of unknowns arise when the problem is approximated. Nevertheless, DFM is shown to be an accurate tool to describe the flow characteristics of the models with large-scale fractures. In another approach, called the embedded fracture model (EFM) (Hajibeygi et al. 2011; Tene et al. 2016a; Ţene et al. 2016b) the fractures are not resolved by grid but are considered as an overlaying continua. In EFM, matrix and fracture are viewed as two porosity types co-existing at the same spatial location, thus simple structured meshes can be used for the domain discretization. The transfer term between matrix and fracture appears as an additional source or sink and is assumed to exist in entire simulation domain. The concept of this approach can be classified in the class of dual-continuum or multi-continuum models (Barenblatt et al. 1960; Warren and Root 1963; Douglas Jr. and Arbogast 1990; Ginting et al. 2011).

In this work, we consider both embedded and discrete fracture models (EFM and DFM) for fine-scale model. Mathematical models for both approaches are described by the coupled mixed dimensional system. Finite volume methods are widely used discretization techniques for simulation of flow problems. For fine grid simulations, we employ the cell-centered finite-volume method with two-point flux approximation (TPFA) (Hajibeygi et al. 2011; Tene et al. 2016a; Ţene et al. 2016b, 2017; Bosma et al. 2017). In the DFM approach, we impose Robin type conditions on the internal boundaries that represent fractures. This allows us to couple the subdomains by simply discretizing the flux over faces of each internal boundary. In the EFM approach, a coupling between fracture and matrix subdomains is described by some transfer term.

Due to the scale disparity, fine grid simulation of the processes in fractured porous media can be very expensive if one needs to capture various scales of flow features at once. To reduce the dimension of the fine scale system directly using finite volume approximation of the problem with EFM and DFM approaches, multiscale methods or upscaling techniques are proposed (Hou and Wu 1997; Efendiev and Hou 2009; Weinan et al. 2007; Lunati and Jenny 2006; Jenny et al. 2005). In our previous work, the multiscale model reduction techniques based on the Generalized multiscale finite element method (GMsFEM) for flow in fractured porous media are presented (Akkutlu

et al. 2015, 2018; Chung et al. 2017; Efendiev et al. 2015). The general idea of GMsFEM is to first solve some local problems to get snapshot spaces, then design suitable spectral problems to obtain important modes which can be used to construct multiscale basis (Efendiev et al. 2012, 2013; Chung et al. 2015, 2016b). The resulting multiscale space contains basis functions that take into account the microscale heterogeneities, and the multiscale scale solution found in this space provide an accurate approximation. Recently, the authors in Chung et al. (2018b) proposed a new GMsFEM method with constraint energy minimization (CEM-GMsFEM). In CEM-GMsFEM, one constructs multiscale basis functions which can capture long channelized effects and can be localized in an oversampling domain. The construction of the multiscale space starts with an auxiliary space, which consists of eigenfunctions of local spectral problems. Using the auxiliary space, one can obtain the required multiscale spaces by solving a constraint energy minimization problem. Using the multiscale basis functions, we recently presented a non-local multi-continuum (NLMC) method (Chung et al. 2018a) for problems in heterogeneous fractured media. We remark that since the local solutions are computed in an oversampled domain, the mass transfers between fractures and matrix become non-local, and the resulting upscaled model contains more effective properties of the flow problem.

In this paper, we construct the multicontinuum upscaled models based on NLMC. We construct multiscale basis functions in each local domain for both fractures and matrix. Upscaled model have only one additional coarse degree of freedom (DOF) for each fracture network. Numerical results show that the coupled NLMC method for the fractured porous media provide accurate and efficient upscaled model on the coarse grid. The implementation is based on the open-source library FEniCS, where we use geometry objects and the FEniCS interface to the linear solvers (Logg 2009; Logg et al. 2012).

This paper is organized as follows. In Sect. 2, we consider mathematical model and present finite volume fine grid approximation for the EFM and DFM approaches. In Sect. 3, we propose an upscaled coarse-grid model for flow in fractured porous media. After that, we present some numerical examples for various model problems, and we show that proposed method can achieve a good accuracy with a very few degrees of freedom and discuss the details in Sects. 4, 5 and 6. A conclusion is drawn in Sect. 7.

2 Problem formulation and fine-grid approximation

In this paper, we consider a common approach based on the mixed dimensional mathematical model for the fractured porous medium (Martin et al. 2005; D'Angelo and Scotti 2012; Formaggia et al. 2014; D'angelo and Quarteroni 2008; Schwenck et al. 2015). Let $\Omega \in \mathcal{R}^d$ (d = 2,3) be the porous matrix domain and $\gamma \in \mathcal{R}^{d-1}$ be the lower dimensional domain for fractures. We consider the following mixed dimensional mathematical model

$$\begin{aligned} a_m \frac{\partial p_m}{\partial t} - \nabla \cdot (b_m \nabla p_m) + r_{mf}(p_m, p_f) &= f_m, \quad x \in \Omega, \\ a_f \frac{\partial p_f}{\partial t} - \nabla \cdot (b_f \nabla p_f) - r_{fm}(p_m, p_f) &= f_f. \quad x \in \gamma, \end{aligned} \tag{1}$$

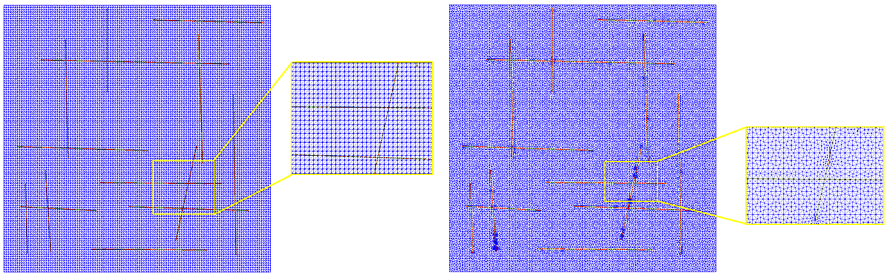

Fig. 1 Computational grids for EFM (left) and DFM (right)

where p_m is the pressure in the porous matrix Ω; p_f is the pressure in the fractures γ; a_m, a_f, b_m and b_f are the problem coefficients (a_m and a_f are constants for simplicity); r_{fm} and r_{fm} are the coupling terms between the fractures and matrix (mass transfer); f_m and f_f are the source terms.

For the fine-grid approximation of the mixed dimensional coupled problem, we use a finite volume method. Approximations of the coupling terms are depends on the type of grid construction, where for the of conforming fracture and porous matrix grids, we use a discrete fracture model, otherwise we use an embedded fracture model. Discrete fracture model (DFM) is associated with unstructured grids with explicit meshing of the fracture geometry, where the fractures are located at the interfaces between matrix cells (Hoteit and Firoozabadi 2008; Karimi-Fard et al. 2003; Karimi-Fard and Firoozabadi 2001; Garipov et al. 2016; Bosma et al. 2017). In embedded discrete fracture model (EDFM), the fracture mesh is not conformed with porous matrix mesh and structured grid can be used (Lee et al. 2001; Li et al. 2006; Hajibeygi et al. 2011; Ţene et al. 2016b, 2017; Tene et al. 2016a).

Let $\mathcal{T}_h = \cup_{i=1}^{N_f^m} \varsigma_i$ be the fine mesh of the domain Ω and let $\mathcal{E}_\gamma = \cup_{l=1}^{N_f^f} \iota_l$ be the fracture fine mesh of the domain γ, where N_f^f and N_f^m are the number of elements in fine grids $\mathcal{E}_\gamma$ and $\mathcal{T}_h$ (see Fig. 1, where the fine grid mesh $\mathcal{T}_h$ is depicted by a blue color and the fracture mesh $\mathcal{E}_\gamma$ by a red color). We note that, the coupling terms r_{mf} and r_{fm} are zero if $\iota_l \cup \varsigma_i = 0$. For time discretization, we use implicit scheme, where $\check{p}_{m,i}$, $\check{p}_{f,l}$ are the solutions from previous time step and τ is the given time step.

Discrete fracture model approximation Let $\mathcal{T}_h$ be the unstructured fine mesh containing triangular or tetrahedral elements that are conforming with fractures, and let $\mathcal{E}_h$ be all fine-scale facets of the mesh $\mathcal{T}_h$. Denote by $\mathcal{E}_\gamma$ the fracture facets, where $\mathcal{E}_\gamma \subset \mathcal{E}_h$ (see right of Fig. 1). For discrete fracture model, we have the following discrete problem using two-point flux approximation

$$a_m \frac{p_{m,i} - \check{p}_{m,i}}{\tau} |\varsigma_i| + \sum_{E_{ij} \subset \partial K_i / \mathcal{E}_\gamma} T_{ij}(p_{m,i} - p_{m,j})$$
$$+ \sum_{\iota_l} \sigma_{il}(p_{m,i} - p_{f,l}) = f_{m,i}|\varsigma_i|, \quad \forall i = 1, N_f^m$$

$$a_f \frac{p_{f,l} - \check{p}_{f,l}}{\tau} |\iota_l| + \sum_n W_{ln}(p_{f,l} - p_{f,n}) - \sum_{\varsigma_i} \sigma_{il}(p_{m,i} - p_{f,l}) = f_{f,l}|\iota_l|, \quad \forall l = 1, N_f^f \tag{2}$$

where $T_{ij} = b_{m,ij}|E_{ij}|/d_{ij}^m$ ($|E_{ij}|$ is the length of facet between cells ς_i and ς_j, d_{ij}^m is the distance between midpoint of cells ς_i and ς_j, $b_{m,ij}$ is the harmonic average between $b_{m,i}$ and $b_{m,j}$), $W_{ln} = b_{f,ln}/d_{ln}^f$ (d_{ln}^f is the distance between midpoint of cells ι_l and ι_n, $b_{f,ln}$ is the harmonic average between $b_{f,l}$ and $b_{f,n}$). Here for mass transfer tems r_{mf} and r_{fm} in Eq. (1), we use a linear approximations with $\sigma_{il} = k_{il}^*|\iota_l|/d_{il}^{mf}$ if $\mathcal{E}_\gamma \cap \partial\varsigma_i = \iota_l$ and zero else (d_{ij}^{mf} is the distance between midpoint of cells ς_i and ι_l, k_{il}^* is the harmonic average between $b_{m,i}$ and $b_{f,l}$).

Note that, the discrete fracture approximation can be used for fluid flow simulation in a fractured porous medium with both high and low permeable fracturesm.

Embedded fracture model approximation Let $\mathcal{T}_h$ be the structured fine grid with triangular or tetrahedral cells of the domain Ω, we note that in this approach the mesh does not need to be conforming with the fracture lines. The additional fracture mesh denoted by $\mathcal{E}_\gamma$ and only performed on the fractures (see left of Fig. 1). For embedded fracture model, we have

$$\begin{aligned} &a_m \frac{p_{m,i} - \check{p}_{m,i}}{\tau} |\varsigma_i| + \sum_{E_{ij} \in \partial K_i} T_{ij}(p_{m,i} - p_{m,j}) \\ &\quad + \sum_{\iota_l} \sigma_{il}(p_{m,i} - p_{f,l}) = f_{m,i}|\varsigma_i|, \quad \forall i = 1, N_f^m \\ &a_f \frac{p_{f,l} - \check{p}_{f,l}}{\tau} |\iota_l| + \sum_n W_{ln}(p_{f,l} - p_{f,n}) \\ &\quad - \sum_{\varsigma_i} \sigma_{il}(p_{m,i} - p_{f,l}) = f_{f,l}|\iota_l|, \quad \forall l = 1, N_f^f \end{aligned} \tag{3}$$

where for mass transfer tems r_{mf} and r_{fm} in Eq. (1), we use a linear approximations with $\sigma_{il} = CI_{il}k_{il}^*$ if $\iota_l \subset \varsigma_i$ and zero else (CI_{il} is the connectivity index from Hajibeygi et al. (2011), Chai et al. (2018) that proportional to the distance and area of the intersection between the fracture cell ι_l and porous matrix cell ς_i, k_{il}^* is the harmonic average between $b_{m,i}$ and $b_{f,l}$).

In implementation of the EDFM, we set fracture as a source term inside cell that can handle high permeable fractures accurately. For accurate approximation of the low permeable fractures, for example, we can introduce additional degrees of freedoms for porous matrix cell, when fracture split matrix cell into several subcells. Very interesting projection based approach is presented in Ţene et al. (2017). In this work, we implemented only the simplest case for EDFM fine grid approximation. Main goal of paper is to show that presented coarse grid method is general, can handle any fine

grid approximations and can be used for low and high permeable fractures on the coarse grid.

Matrix form Therefore, we have the following system of equations for $p = (p_m, p_f)^T$ presented in the matrix form

$$M\frac{p-\check{p}}{\tau} + (A+Q)p = F,$$
$$M = \begin{pmatrix} M_m & 0 \\ 0 & M_f \end{pmatrix}, \quad A = \begin{pmatrix} A_m & 0 \\ 0 & A_f \end{pmatrix}, \quad Q = \begin{pmatrix} Q_m & Q_{fm}^T \\ Q_{fm} & Q_f \end{pmatrix}, \quad F = \begin{pmatrix} F_m \\ F_f \end{pmatrix}, \quad (4)$$

and

$$M_m = \{m_{ij}^m\}, \quad m_{ij}^m = \begin{cases} a_m|\varsigma_i| & i = j, \\ 0 & i \neq j \end{cases}, \quad M_f = \{m_{ln}^f\}, \quad m_{ln}^f = \begin{cases} a_f|\iota_l| & l = n, \\ 0 & l \neq n \end{cases},$$
$$A_m = \{a_{ij}^m\}, \quad a_{ij}^m = \begin{cases} \sum_j T_{ij} & i = j, \\ -T_{ij} & i \neq j \end{cases}, \quad A_f = \{a_{ln}^f\}, \quad a_{ln}^f = \begin{cases} \sum_n W_{ln} & l = n, \\ -W_{ln} & l \neq n \end{cases},$$
$$Q_m = \{q_{ij}^m\}, \quad q_{ij}^m = \begin{cases} \sum_l \sigma_{il} & i = j, \\ 0 & i \neq j \end{cases}, \quad Q_f = \{q_{ln}^f\}, \quad q_{ln}^f = \begin{cases} \sum_i \sigma_{il} & l = n, \\ 0 & l \neq n \end{cases},$$
$$Q_{fm} = \{q_{li}^{fm}\}, \quad q_{li}^{fm} = \begin{cases} -\sigma_{li} & \mathcal{E}_\gamma \cap \partial\varsigma_i = \iota_l (\text{DFM}) \text{ or } \iota_l \subset \varsigma_i (\text{EFM}), \\ 0 & \text{else} \end{cases},$$

where $F_m = \{f_i^m\}$, $f_i^m = f_{m,i}|\varsigma_i|$, $F_f = \{f_l^f\}$, $f_l^f = f_{f,l}|\iota_l|$. We note that $\sum_j a_{ij} = 0$ and $\sum_j q_{ij} = 0$ where we denote $A = \{a_{ij}\}$ and $Q = \{q_{ij}\}$. Here A_m, M_m, Q_m have size $N_f^m \times N_f^m$; A_f, M_f, Q_f have size $N_f^f \times N_f^f$; Q_{fm} have size $N_f^f \times N_f^m$ and A and M are an $N_f \times N_f$ matrices, where $N_f = N_f^m + N_f^f$ and $N_f^m \neq N_f^f$.

Note that, the size of the resulting system even after EDFM or DFM approaches is beyond the scope of classical simulation methods presented in this Section Ţene et al. (2016b), Praditia et al. (2018). In general, EDFM method can be used on a coarse grid as an upscaling method for the cases with homogeneous permeability and high permeable fractures. For the heterogeneous permeability, EDFM should be coupled with some upscaling technique. For low conductive fractures, an extension of the method should be implemented (pEDFM). However, even for a homogeneous case, a classical upscaling using EDFM on the coarse grid leads to the inaccurate simulations (Praditia et al. 2018). Therefore, for dimension reduction of the resulting system with accurate approximations on the coarse grid, a multiscale method should be developed. The main goal of paper is the development of the general coarse grid method using NLMC, that can handle any fine grid approximations, heterogeneous porous matrix properties, and can be used for low and high permeable fractures on the coarse grid.

3 Coarse-grid upscaled method

Next, we describe the construction of the upscaled model on coarse grid using Non-local multi-continuum (NLMC) approach. In this method, the multiscale basis functions are constructed by solving local problems in the oversampled local region. The basis functions satisfy the constraint that it vanishes in all other continuum except for the target continuum which it is formulated for. Construction of basis is similar for both discrete and embedded fine-grid fracture models.

In NLMC Chung et al. (2018a), we apply simplified basis for fractured media to form the auxiliary space, which will be used together with an energy minimization principle for form the required basis functions. The resulting multiscale basis functions have spatial decay property in local domains and separate background medium and fractures. Finally, the basis functions are used in the construction of the upscaled model.

Let K_i^+ be an oversampled region for the coarse cell K_i (see Fig. 2) obtained by enlarging K_i by several coarse cell layers. We will construct a set of basis functions, whose supports are K_i^+. Each of these basis functions is related to the matrix component in K_i as well as each fracture network within K_i. For fractures, we denote $\gamma = \cup_{l=1}^{L} \gamma^{(l)}$, where $\gamma^{(l)}$ denotes the lth fracture network and L is the total number of fracture networks. We also write $\gamma_j^{(l)} = K_j \cap \gamma^{(l)}$ is the fracture inside coarse cell K_j and L_j is the number of fracture networks in K_j. For each K_i, we will therefore obtain $L_j + 1$ basis functions: one for K_i and one for each $\gamma_i^{(l)}$. Following the framework of Chung et al. (2018a,b), the auxiliary space $V^{aux}(K_i)$ for the coarse cell K_i contains functions that are supported in K_i and are piecewise constant functions such that they are constant on K_i and on each $\gamma_i^{(l)}$.

We next define the constraints that will be used for multiscale basis construction. For each $K_j \subset K_i^+$:

(1) background medium (ψ_0^i) :

$$\int_{K_j} \psi_0^i \, dx = \delta_{i,j}, \quad \int_{\gamma_j^{(l)}} \psi_0^i \, ds = 0, \quad l = \overline{1, L_j}.$$

(2) lth fracture network in K_i (ψ_l^i):

$$\int_{K_j} \psi_l^i \, dx = 0, \quad \int_{\gamma_j^{(l)}} \psi_l^i \, ds = \delta_{i,j}\delta_{m,l}, \quad l = \overline{1, L_j}.$$

We first discuss the constraint for background medium in (1). We note that it is a set of constraints so that the resulting function has mean value one on the coarse cell K_i, and has mean value zero on all other coarse cells within K_i^+. In addition, the resulting function has mean value on all fracture networks within K_i^+. We next discuss the constraint for the fracture network (2). We note that it is a set of constraints so that the resulting function has mean value zero on all coarse cells within K_i^+. Moreover, the resulting function has mean value one on the target fracture network $\gamma_i^{(l)}$ and has

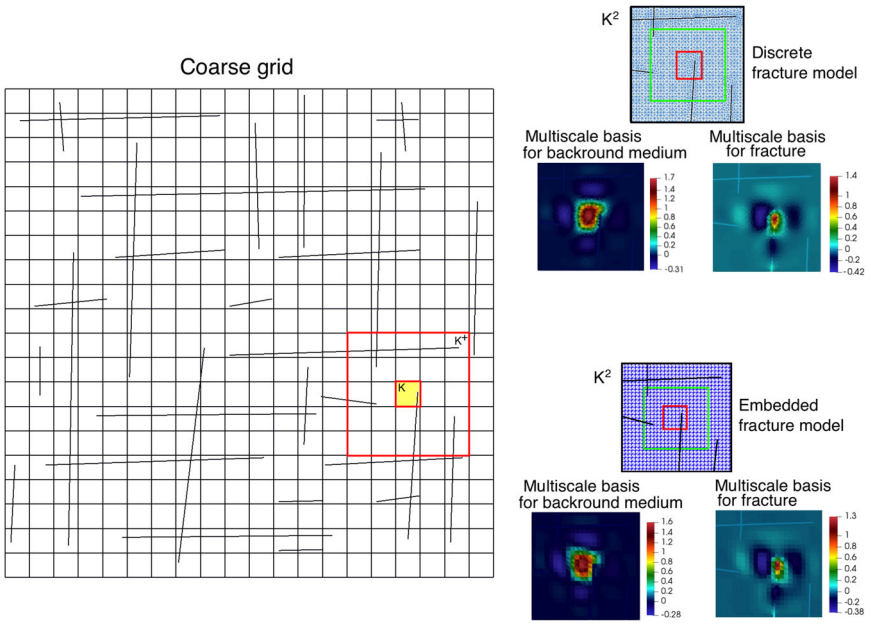

Fig. 2 Multiscale basis functions on mesh 20×20 for local domain K^2 for DFM and EFM fine-grid approximations

mean value zero on all fracture networks within K_i^+. To sum up, the above constraints will give $L_i + 1$ functions.

Together with the above constraints, we will construct the basis functions as follows. Following the framework of Chung et al. (2018a, b), we will find the multiscale basis functions using the energy minimizing constraint property. As a result, we will solve the following local problems in the oversampled region K_i^+ using a fine-grid approximation for the system of flow in fractured porous media presented in the previous Section. In particular, we solve following coupled system in K_i^+:

$$\begin{pmatrix} A_m + Q_m & Q_{fm}^T & B_m^T & 0 \\ Q_{fm} & A_f + Q_f & 0 & B_f^T \\ B_m & 0 & 0 & 0 \\ 0 & B_f & 0 & 0 \end{pmatrix} \begin{pmatrix} \psi_m \\ \psi_f \\ \mu_m \\ \mu_f \end{pmatrix} = \begin{pmatrix} 0 \\ 0 \\ F_m \\ F_f \end{pmatrix} \tag{5}$$

with zero Dirichlet boundary conditions on ∂K_i^+ for ψ_m and ψ_f. There are existing methods for imposing Dirichlet boundary conditions in the discrete system. In this implementation, we use the simplest approach, where we modify system on the degrees of freedoms associated to the boundary cells. For the row that associated to the boundary cell, we set 1 on the diagonal and 0 for off diagonal elements.

We remark that (ψ_m, ψ_f) denotes each of the basis functions that satisfy the above constraints. Note that we used Lagrange multipliers μ_m and μ_f to impose the constraints in the multiscale basis construction. To construct multiscale basis function

with respect to porous matrix $\psi^0 = (\psi_m^0, \psi_f^0)$, we set $F_m = \delta_{i,j}$ and $F_f = 0$. For multiscale basis function with respect to the lth fracture network, we set $F_m = 0$ and $F_f = \delta_{i,j}\delta_{m,l}$. In Fig. 2, we depict a multiscale basis functions for oversampled region $K_i^+ = K_i^2$ (two oversampling coarse cell layers) in a 20×20 coarse mesh.

Remark 1 For the multiscale basis functions construction for the time-dependent problems, we can use matrix $(\frac{1}{\tau}M + A + Q)$ instead of $(A + Q)$ Mehmani and Tchelepi (2019). This leads to the time step size dependent local problems and will be considered in future works.

Combining these multiscale basis functions, we obtain the following multiscale space

$$V_{ms} = \text{span}\{(\psi_m^{i,l}, \psi_f^{i,l}),\ i = \overline{1, N_c},\ l = \overline{0, L_i}\}$$

and the projection matrix

$$\begin{aligned}
R &= \begin{pmatrix} R_{mm} & R_{mf} \\ R_{fm} & R_{ff} \end{pmatrix}, \\
R_{mm}^T &= \left[\psi_m^{0,0}, \psi_m^{1,0} \dots \psi_m^{N_c,0}\right], \\
R_{ff}^T &= \left[\psi_f^{0,1} \dots \psi_f^{0,L_0}, \psi_f^{1,1} \dots \psi_f^{1,L_1}, \dots, \psi_f^{N_c,1} \dots \psi_f^{N_c,L_{N_c}}\right], \\
R_{mf}^T &= \left[\psi_f^{0,0}, \psi_f^{1,0} \dots \psi_f^{N_c,0}\right], \\
R_{fm}^T &= \left[\psi_m^{0,1} \dots \psi_m^{0,L_0}, \psi_m^{1,1} \dots \psi_m^{1,L_1}, \dots, \psi_m^{N_c,1} \dots \psi_m^{N_c,L_{N_c}}\right],
\end{aligned}$$

Therefore, the resulting upscaled coarse grid model reads

$$\bar{M}\frac{\bar{p}^{n+1} - \bar{p}^n}{\tau} + (\bar{A} + \bar{Q})\bar{p}^{n+1} = \bar{F}, \tag{6}$$

where $\bar{A} = RAR^T$, $\bar{M} = RMR^T$, $\bar{Q} = RQR^T$, $\bar{F} = RF$ and $\bar{p} = (\bar{p}_m, \bar{p}_f)^T$. We remark that $\bar{p}_m$ and $\bar{p}_f$ are the average cell solution on coarse grid element for background matrix and for fracture media. That is, each component of $\bar{p}_m$ corresponds to the mean value of the solution on each coarse cell. Moreover, each component of $\bar{p}_f$ corresponds to the mean value of the solution on each fracture network with a coarse cell.

Due to the constrains that we used for the multiscale basis functions construction, we can use diagonal mass matrices directly calculated on the coarse grid. We remark that the matrix A is non-local and provide good approximation due to the basis construction.

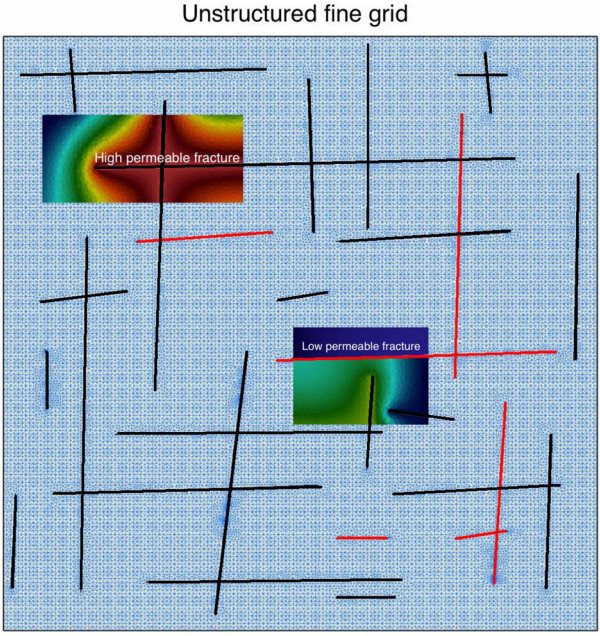

Fig. 3 Discrete fracture model with low and high permeable fractures. Blue: fine grid. Black: high permeable fractures. Red: low permeable fractures

4 Numerical results for high and low permeable fractures with DFM

In this section, we consider low and high permeable fractures (see Fig. 3 for illustration). We construct an accurate approximation of the pressure equation using NLMC approach. The ideas to construct the basis are similar for low and high permeable fracture cases, where only the underlying fine grid models are different. In Fig. 2, we depict multiscale basis functions in an oversampled local domain K^2 on a 20×20 coarse mesh (Fig. 4).

We consider the computational domain $\Omega = [0, 1] \times [0, 1]$ with 30 fractures. In Fig. 5, we show the coarse and fine grids. For fine-grid models, we use DFM, thus the fractures are resolved by the fine grid. The coarse grids are uniformly partitioned into 20×20 and 40×40 coarse blocks. In general, coarse grid can have an any shapes of cells (unstructured coarse grid) (Bosma et al. 2017; Chung et al. 2016a). In this work, for simplicity, we focus only on structured coarse grids, where we construct an unstructured fine grid that conforming with coarse grid edges.

We consider three test cases:

- Test 1 (high permeable fractures). $k_m = 10^{-6}$, $k_f = 1.0$ for all fractures.
- Test 2 (low permeable fractures). $k_m = 10^{-4}$, $k_f = 10^{-10}$ for all fractures.
- Test 3 (hybrid fractures). $k_m = 10^{-6}$, $k_f = 1.0$ for 24 fractures and $k_f = 10^{-12}$ for 6 fractures.

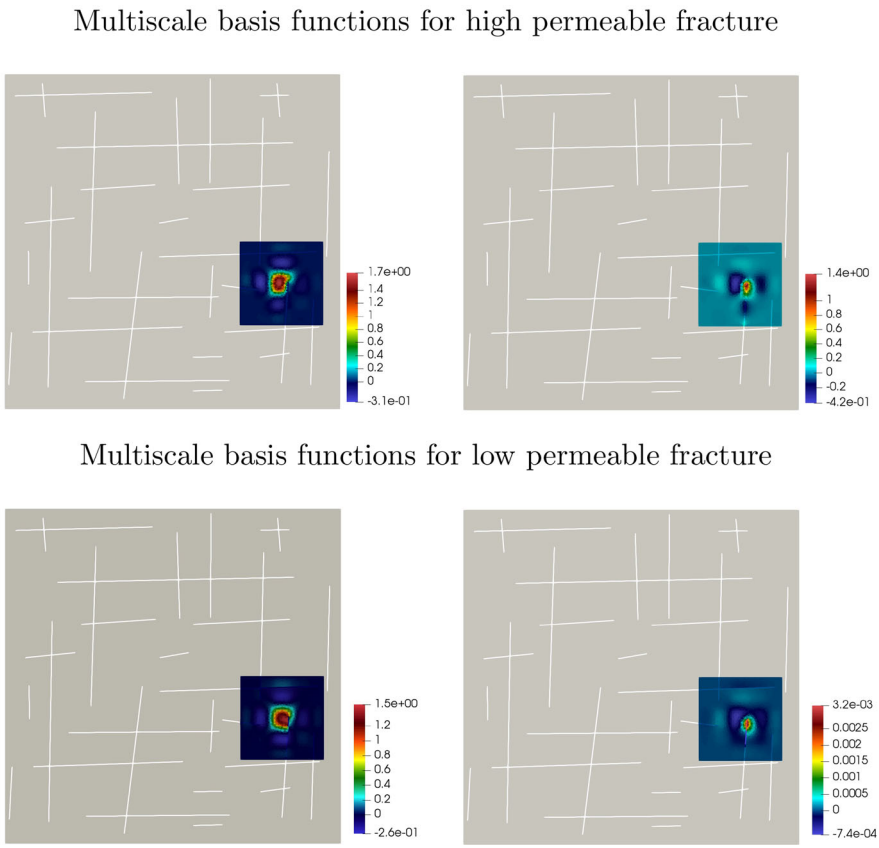

Fig. 4 Multiscale basis functions on a 20×20 mesh for local domain K^2. First row: multiscale basis functions for matrix and high permeable fracture. Second row: multiscale basis functions for matrix and low permeable fracture. Left column: multiscale basis functions for matrix. Right column: multiscale basis functions for fracture

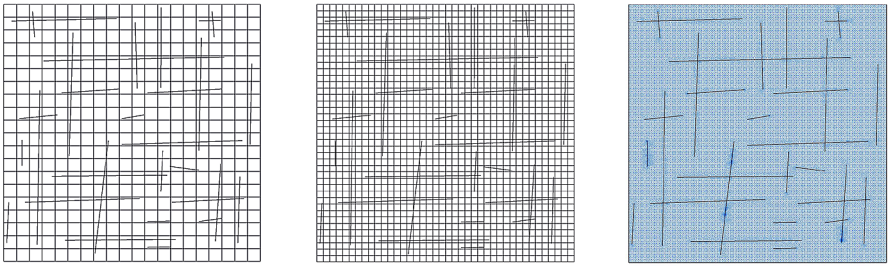

Fig. 5 Computational grids. Coarse grids with 400 and 1600 cells. Fine grid with 47,520 elements (matrix) and 1042 elements (fractures)

The other model parameters are chosen as follows: $c_m = 10^{-5}$, $c_f = 10^{-6}$ with $\sigma = \frac{2.0}{k_m^{-1} + k_f^{-1}}$.

Table 1 Relative errors (%) of the mean solution on a coarse mesh 20×20 (left) and 40×40 (right); Test 1, 2 and 3

K^s	t_5	t_{10}	t_{15}	t_{20}	K^s	t_5	t_{10}	t_{15}	t_{20}
Test 1. 20×20					Test 1. 40×40				
$s = 1$	0.569	1.147	1.740	2.307	$s = 1$	0.600	1.164	1.695	2.175
$s = 2$	0.233	0.246	0.263	0.283	$s = 2$	0.162	0.255	0.326	0.383
$s = 3$	0.229	0.236	0.254	0.272	$s = 3$	0.151	0.202	0.231	0.248
Test 2. 20×20					Test 2. 40×40				
$s = 1$	–	–	–	–	$s = 1$	–	–	–	–
$s = 2$	0.862	2.780	6.183	11.990	$s = 2$	0.429	1.118	2.068	3.271
$s = 3$	0.095	0.151	0.191	0.224	$s = 3$	0.072	0.122	0.162	0.195
Test 3. 20×20					Test 3. 40×40				
$s = 1$	0.793	1.891	3.108	4.319	$s = 1$	0.839	1.751	2.699	3.610
$s = 2$	0.323	0.395	0.432	0.451	$s = 2$	0.215	0.348	0.442	0.523
$s = 3$	0.311	0.382	0.427	0.446	$s = 3$	0.207	0.331	0.419	0.476

We set a source $q = 10^{-3}$ on the fractures in the two coarse cells,

- Test 1 and 3. cell: $0.1 < x < 0.15, 0.05 < y < 0.1$ and cell: $0.6 < x < 0.65, 0.9 < y < 0.95$.
- Test 2. cell: $0.05 < x < 0.1, 0.05 < y < 0.1$ and cell: $0.65 < x < 0.7, 0.9 < y < 0.95$.

As for initial pressure, we set $p_0 = 1$. Our total simulation time is $t_{max} = 0.1$, and we take 20 time steps for upscaled and fine-scale solvers.

To compare the results, we investigate the relative L^2 error between coarse cell average of the fine-scale solution $\bar{p}_f$ and upscaled coarse grid solutions $\bar{p}$

$$e_{L_2} = \sqrt{\frac{\sum_K (\bar{p}_f^K - \bar{p}^K)^2}{\sum_K (\bar{p}_f^K)^2}} \cdot 100, \quad \bar{p}_f^K = \frac{1}{|K|} \int_K p_f \, dx. \tag{7}$$

The fine-scale system has dimension $DOF_f = 47520 + 1042$. The upscaled model has dimension $DOF_c = 593$ for coarse mesh with 400 cells (20×20, and $DOF_c = 1965$ for coarse mesh with 1600 cells (40×40). In Fig. 6, we present the fine scale solution for all test cases at different time steps $t_5 = 0.025, t_{10} = 0.05, t_{15} = 0.075$ and $t_{20} = 0.1$. The first row present solutions for Test 1, where we have highly conductive fractures. The second row show the solutions for the low permeable fractures. Finally, in the third row we depict solutions where the fractures have both high and low permeability.

In Fig. 7, we present the upscaled solutions for coarse grid 40×40 for Test 1, 2 and 3. For basis calculations, we use oversampled domain K^+ with 3 coarse cells layers oversampling. We observe good accuracy of the proposed method with less than 1% of error for all test cases.

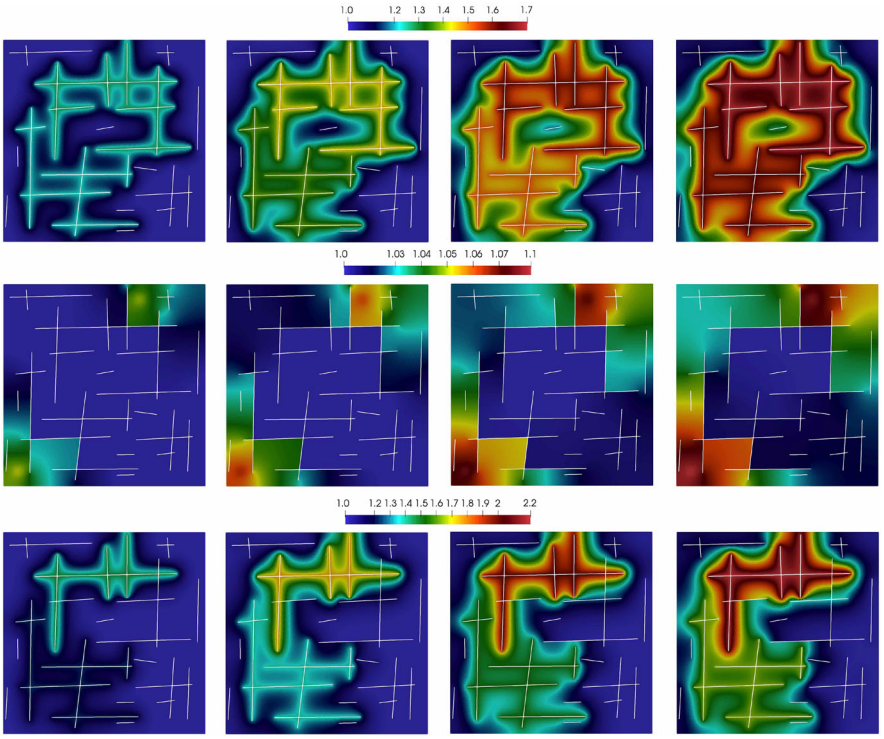

Fig. 6 Fine-scale solutions for Tests 1,2 and 3 (from top to bottom) for different time steps $t_5 = 0.025$ (first column), $t_{10} = 0.05$ (second column), $t_{15} = 0.075$ (third column) and $t_{20} = 0.1$ (fourth column). $DOF_f = 48{,}562$

In Table 1, we present relative errors for two coarse grids and for different numbers of oversampling layers K^s with $s = 1, 2$ and 3. We notice a huge reduction of the system dimension and very small errors for unsteady mixed dimensional coupled system.

Our method provides good results for the use of sufficient number of oversampling layers (Chung et al. 2018b). From Tables 1, 2 and 3, we observe that one oversampling layer is not enough for obtaining good results, but we observe accurate solution when we take two or more oversampling layers (see Fig. 8 for illustration). For example in Test 1 and 3, we observe that two oversampling layers is enough to get good results, but in Test 2 we should use three oversampling layers. On the other hand, we should take a minimal number of oversampling layers because number of layers directly effects to the sparsity of the matrix due to nonlocal connections in the stiffness matrix and effects to the time of multiscale basis calculations. For example, in Test 1 for finite volume approximation with DFM, we have approximately $nnz_f \approx 195{,}000$ and $DOF_f = 48{,}562$ on the fine grid (nnz be denoted the number of nonzero elements in matrix). In NLMC, we have $DOF_c = 593$ for 20×20 coarse grid, where $nnz_c = 17{,}073$ for $s = 1$ (4.85% of elements for 593×593 matrix), $nnz_c = 27{,}989$ for $s = 2$ (7.95% of elements) and $nnz_c = 29711$ for $s = 3$ (8.44% of elements). We note that, we

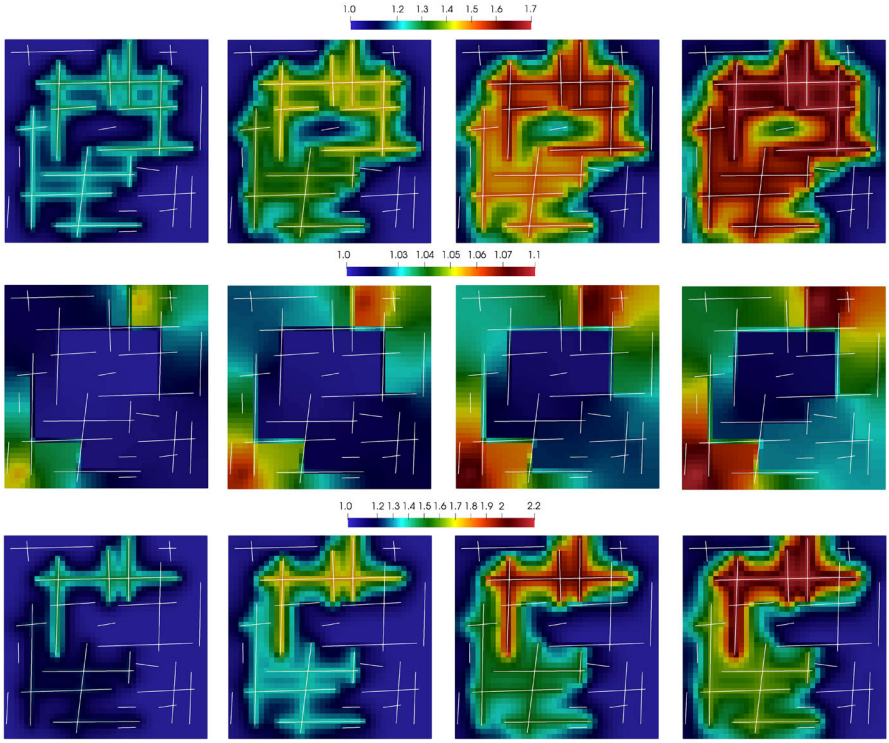

Fig. 7 Upscaled coarse grid solutions on mesh 40×40 with K^3 for different time steps $t_5 = 0.025$ (first column), $t_{10} = 0.05$ (second column), $t_{15} = 0.075$ (third column) and $t_{20} = 0.1$ (fourth column). Tests 1,2 and 3 (from top to bottom). $DOF_c = 1965$

construct mass matrices and right-hand side vectors directly on the coarse grid, and for matrix $\bar{A} = RAR^T$ elements, we use a threshold with $\epsilon = 10^{-8}$ for preserving sparsity.

5 Numerical results with EFM

In this section, we present numerical results for upscaled model for embedded and discrete fine-grid fracture models. We consider highly permeable fractures for two types of geometries. As for Geometry 1, we consider 30 fracture lines in the domain (Test 1 from the previous section) with injection and production wells (Fig. 5). Geometry 2 is the computational domain $\Omega = [0, 2] \times [0, 1]$ with 50 fractures (Fig. 9).

We set a source term on the fractures inside following cells:

- Geometry 1. Cell $0.1 < x < 0.15, 0.05 < y < 0.1$ (injection) and cell $0.6 < x < 0.65, 0.9 < y < 0.95$ (production) with $q = \pm 10^{-3}$.
- Geometry 2. Cells $0.1 < x < 0.15, 0.05 < y < 0.1$ and $1.6 < x < 1.65, 0.9 < y < 0.95$ for injection with $q = 10^{-3}$.

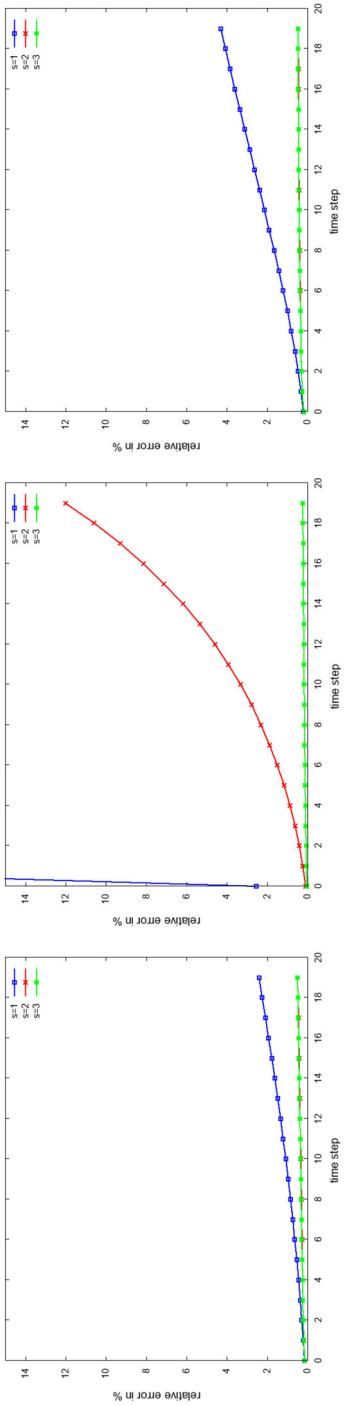

Fig. 8 Relative errors (%) of the mean solution on a coarse mesh 20×20. Test 1, 2 and 3 (from left to right)

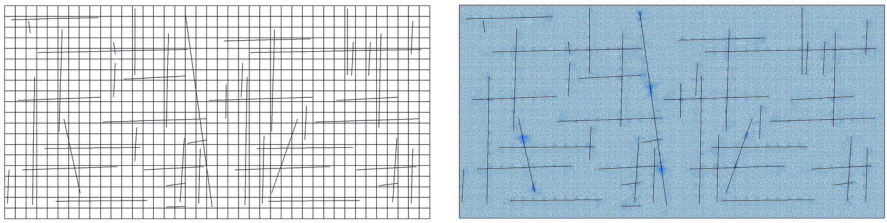

Fig. 9 Computational grids. Coarse grid with 800 cells. Fine grid with 98,398 cells (matrix) and 2170 cells (fractures) (DFM). *Geometry 2*

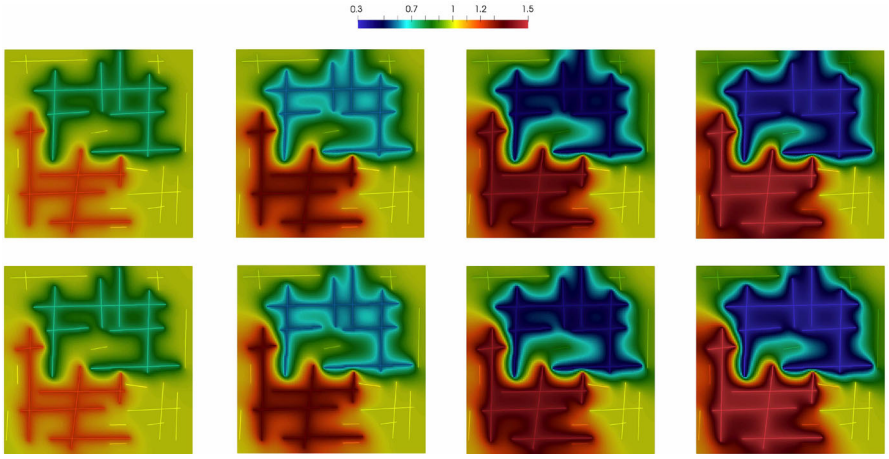

Fig. 10 EFM and DFM fine-scale solutions. Geometry 1 for different time steps $t_5 = 0.025$ (first column), $t_{10} = 0.05$ (second column), $t_{15} = 0.075$ (third column) and $t_{20} = 0.1$ (fourth column). First row: DFM fine-scale solution. Second row: EFM fine-scale solution

The total simulation time is $t_{max} = 0.1$, and is discretized into 20 time steps for both upscaled and fine-scale solvers.

We first consider Geometry 1. For DFM model, the unstructured fine grid contains 47520 fine-scale elements for porous matrix and 1042 fine-scale elements for fractures. For EFM model, we use the structured fine grid containing 20,000 fine-scale elements (matrix) and 1042 fine-scale elements (fractures). We consider uniformly structured coarse grid with 400 coarse-scale elements(20×20). Fine-grid solutions using DFM and EFM models are presented in Fig. 10. We notice similar solutions for both models for sufficient fine grids.

In Table 2, we show relative errors for different number of oversampling layers K^s with $s = 1, 2$ and 3, using DFM and EFM fine grid approximations. For coarse mesh with 400 cells, when we take 2 oversampling layers, we have 0.398% of error at final time. The fine-scale systems have $DOF_f = 47{,}520 + 1042$ for DFM and $DOF_f = 20{,}000 + 1042$ for EFM. While the upscaled model only has $DOF_c = 593$ for coarse mesh with 400 cells (20×20). We note that our proposed method provide with huge reduction of the system size and very accurate approximations.

Table 2 Relative errors (%) of the average cell solution on a coarse mesh. Right: DFM. Left: EFM. Geometry 1 and 2

K^s	t_5	t_{10}	t_{15}	t_{20}	K^s	t_5	t_{10}	t_{15}	t_{20}
Geometry 1 with DFM. 20×20					Geometry 1 with EFM. 20×20				
$s = 1$	0.433	0.955	1.623	2.404	$s = 1$	0.380	0.724	1.127	1.578
$s = 2$	0.233	0.314	0.396	0.476	$s = 2$	0.264	0.390	0.499	0.598
$s = 3$	0.201	0.305	0.378	0.455	$s = 3$	0.259	0.388	0.483	0.579
Geometry 2 with DFM. 40×20					Geometry 2 with EFM. 40×20				
$s = 1$	–	–	–	–	$s = 1$	–	–	–	–
$S = 2$	0.225	0.311	0.375	0.414	$s = 2$	0.430	0.543	0.602	0.627
$s = 3$	0.161	0.185	0.197	0.204	$s = 3$	0.354	0.427	0.466	0.466

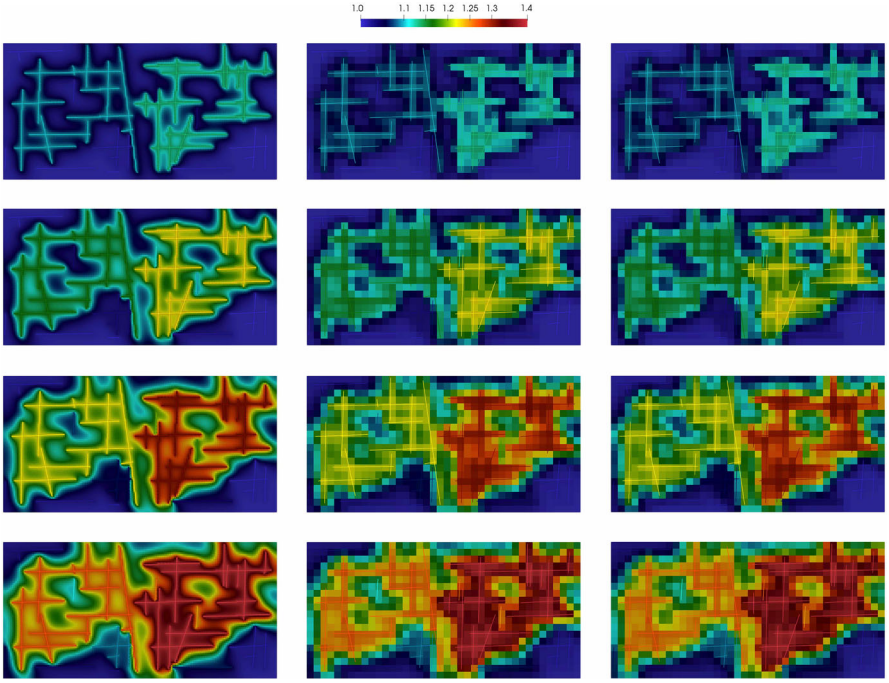

Fig. 11 Multiscale solutions on mesh 40×20 with K^2 using EFM fine-scale solver. Geometry 2 for different time steps $t_5 = 0.025$, $t_{10} = 0.05$, $t_{15} = 0.075$ and $t_{20} = 0.1$ (from top to bottom). First column: fine scale solution. Second column: cell average for fine grid solution. Third column: upscaled coarse grid solution

Next, we consider Geometry 2. For DFM model, we use unstructured fine grid containing 98398 fine cells (matrix) and 2170 fine cells (fractures). For EFM mode, we employ structured fine grid containing 25600 fine cells (matrix) and 2170 fine cells (fractures). In this test, we consider uniform structured coarse grids 40×20 (800 cells). The fine-scale systems have $DOF_f = 98{,}398 + 2170$ for DFM and $DOF_f = 25{,}600 + 2170$ for EFM. The upscaled model has $DOF_c = 1179$ for

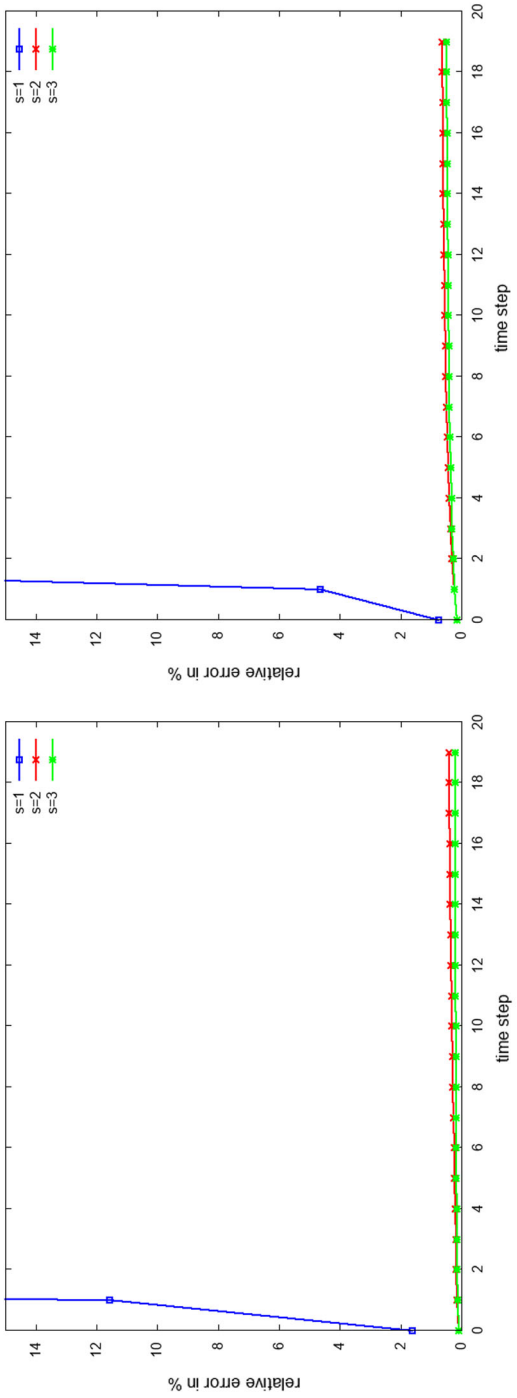

Fig. 12 Relative errors (%) of the average cell solution on a coarse mesh. Right: DFM. Left: EFM. Geometry 2

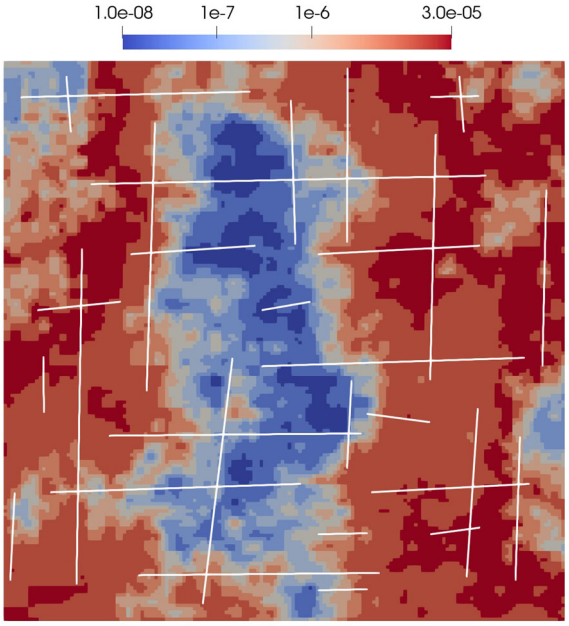

Fig. 13 Heterogeneous pore matrix permeability for Geometry 1

Table 3 Relative errors (%) of the average cell solution on a coarse mesh. Geometry 1 with heterogeneous permeability

K^s	t_5	t_{25}	t_{50}	t_{100}
Geometry 1. 40×40				
$s = 1$	0.137	0.434	0.581	0.785
$s = 2$	0.078	0.182	0.230	0.306
$s = 3$	0.078	0.178	0.200	0.186
$s = 4$	0.078	0.176	0.198	0.183

coarse mesh with 800 cells (40×20). In Fig. 11, we present results using the upscaled model, where we obtain very accurate simulation results with very small DOF in the upscaled model. For local domain K^2, relative error for porous matrix are less than one percent.

In Table 2, we present relative errors between the solutions of EFM and DFM fine-grid models and the upscaled model, where we only use two oversampling layers K^2 for basis construction. From the numerical results, we observe a good convergence when we take sufficient number of oversampled layers (Fig. 12).

6 Numerical results for heterogeneous permeability

Finally, we consider a test case with heterogeneous permeability (Fig. 13) for Geometry 1 with same parameters as in the previous section. As for fine grid approximation, we use EFM. The simulation time is $t_{max} = 0.1$ with 100 time steps.

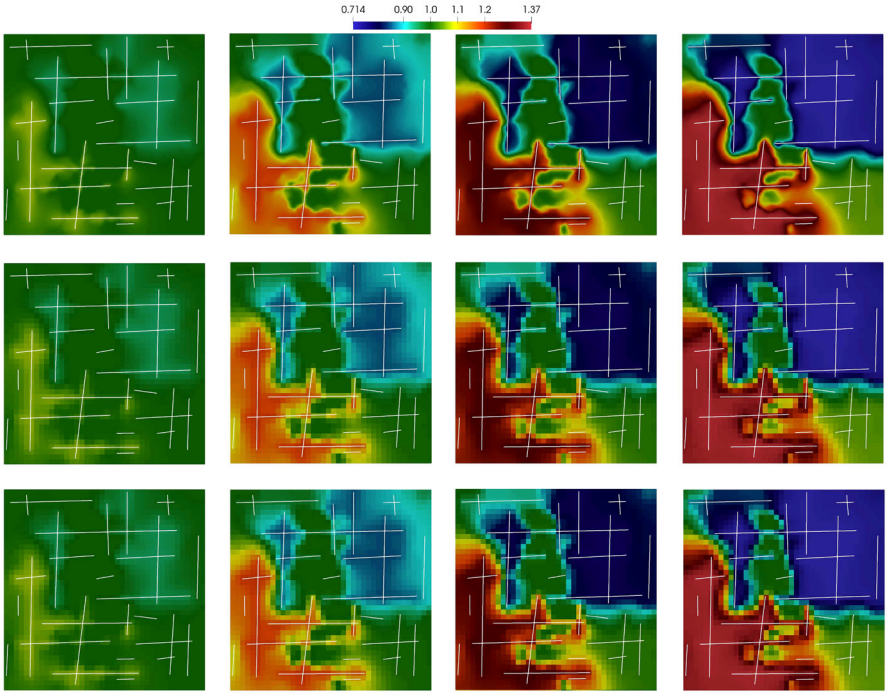

Fig. 14 Multiscale solutions on mesh 40×40 with K^2 using EFM fine-scale solver. Geometry 1 for different time steps t_5, t_{25}, t_{50} and t_{100} (from left to right). First row: fine scale solution. Second row: cell average for fine grid solution. Third row: upscaled coarse grid solution

In this test, we consider uniform structured coarse grids 40×40 (1600 cells). In Fig. 14, we present results using the upscaled model, where relative error are less than one percent. In Table 3, we present relative errors between projection of fine grid solution on a coarse mesh and the upscaled coarse grid solutions. The fine-scale systems have size $DOF_f = 27{,}384$ with solution time 57 s. The upscaled model has $DOF_c = 1165$ with solution time 5.9 s. The computational time is reduced 10 times due to the reduction in the size of the system. The proposed method is shown to be very efficient and provides good accuracy.

7 Conclusion

We consider mixed dimensional coupled problem for flow simulation in fractured porous media for EFM and DFM with finite volume approximation on the fine grid. We presented an upscaling method for coupled problems in fractured domains. In this work, we construct multiscale basis function for background medium and additional multiscale basis for fractures.

We presented numerical results for model problems: (1) discrete fracture fine grid model with low and high permeable fractures; (2) embedded fine grid model for two

geometries with different number of fracture lines and (3) embedded fracture fine grid model with heterogeneous permeability. Our proposed upscaling method provides good accuracy and give a significant reduction in the size of the problem system. The resulting upscaled model has minimal size and the solution obtained has physical meaning on the coarse grid.

Acknowledgements MV's and VA's works are supported by the grant of the Russian Scientific Found N17-71-20055 and the mega-grant of the Russian Federation Government (N 14.Y26.31.0013). EC's work is partially supported by Hong Kong RGC General Research Fund (Project 14304217) and CUHK Direct Grant for Research 2017-18.

References

Akkutlu, I.Y., Efendiev, Y., Vasilyeva, M.: Multiscale model reduction for shale gas transport in fractured media. Comput. Geosci. **20**, 953–973 (2015)

Akkutlu, I.Y., Efendiev, Y., Vasilyeva, M., Wang, Y.: Multiscale model reduction for shale gas transport in poroelastic fractured media. J. Comput. Phys. **353**, 356–376 (2018)

Barenblatt, G.I., Zheltov, I.P., Kochina, I.N.: Basic concepts in the theory of seepage of homogeneous liquids in fissured rocks [strata]. J. Appl. Math. Mech. **24**(5), 1286–1303 (1960)

Bosma, S., Hajibeygi, H., Tene, M., Tchelepi, H.A.: Multiscale finite volume method for discrete fracture modeling on unstructured grids (MS-DFM). J. Comput. Phys. **351**, 145–164 (2017)

Chai, Z., Yan, B., Killough, J.E., Wang, Y.: An efficient method for fractured shale reservoir history matching: the embedded discrete fracture multi-continuum approach. J. Pet. Sci. Eng. **160**, 170–181 (2018)

Chung, E.T., Efendiev, Y., Li, G., Vasilyeva, M.: Generalized multiscale finite element method for problems in perforated heterogeneous domains. Appl. Anal. **255**, 1–15 (2015)

Chung, E.T., Efendiev, Y., Vasilyeva, M., Wang, Y.: A multiscale discontinuous Galerkin method in perforated domains. In: Proceedings of the Institute of Mathematics and Mechanics, vol. 42, pp. 212–229 (2016a)

Chung, E., Efendiev, Y., Hou, T.Y.: Adaptive multiscale model reduction with generalized multiscale finite element methods. J. Comput. Phys. **320**, 69–95 (2016b)

Chung, E.T., Efendiev, Y., Leung, T., Vasilyeva, M.: Coupling of multiscale and multi-continuum approaches. GEM Int. J. Geomath. **8**(1), 9–41 (2017)

Chung, E.T., Efendiev, Y., Leung, W.T., Vasilyeva, M., Wang, Y.: Non-local multi-continua upscaling for flows in heterogeneous fractured media. J. Comput. Phys. **372**, 22–34 (2018a)

Chung, E.T., Efendiev, Y., Leung, W.T.: Constraint energy minimizing generalized multiscale finite element method. Comput. Methods Appl. Mech. Eng. **339**, 298–319 (2018b)

D'angelo, C., Quarteroni, A.: On the coupling of 1d and 3d diffusion-reaction equations: application to tissue perfusion problems. Math. Models Methods Appl. Sci. **18**(08), 1481–1504 (2008)

D'Angelo, C., Scotti, A.: A mixed finite element method for Darcy flow in fractured porous media with non-matching grids. ESAIM Math. Model. Numer. Anal. **46**(2), 465–489 (2012)

Douglas, Jr., J., Arbogast, T.: Dual porosity models for flow in naturally fractured reservoirs. In: Dynamics of Fluids in Hierarchical Porous Media, pp. 177–221 (1990)

Efendiev, Y., Hou, T.: Multiscale Finite Element Methods: Theory and Applications. Surveys and Tutorials in the Applied Mathematical Sciences, vol. 4. Springer, New York (2009)

Efendiev, Y., Galvis, J., Gildin, E.: Local-global multiscale model reduction for flows in highly heterogeneous media. J. Comput. Phys. **231**(24), 8100–8113 (2012)

Efendiev, Y., Galvis, J., Hou, T.: Generalized multiscale finite element methods. J. Comput. Phys. **251**, 116–135 (2013)

Efendiev, Y., Lee, S., Li, G., Yao, J., Zhang, N.: Hierarchical multiscale modeling for flows in fractured media using generalized multiscale finite element method. GEM Int. J. Geomath. **6**(2), 141–162 (2015)

Formaggia, L., Fumagalli, A., Scotti, A., Ruffo, P.: A reduced model for Darcy's problem in networks of fractures. ESAIM Math. Model. Numer. Anal. **48**(4), 1089–1116 (2014)

Garipov, T.T., Karimi-Fard, M., Tchelepi, H.A.: Discrete fracture model for coupled flow and geomechanics. Comput. Geosci. **20**(1), 149–160 (2016)

Ginting, V., Pereira, F., Presho, M., Wo, S.: Application of the two-stage Markov Chain monte carlo method for characterization of fractured reservoirs using a surrogate flow model. Comput. Geosci. **15**(4), 691 (2011)
Hajibeygi, H., Kavounis, D., Jenny, P.: A hierarchical fracture model for the iterative multiscale finite volume method. J. Comput. Phys. **230**(24), 8729–8743 (2011)
Hoteit, H., Firoozabadi, A.: An efficient numerical model for incompressible two-phase flow in fractured media. Adv. Water Resour. **31**(6), 891–905 (2008)
Hou, T., Wu, X.H.: A multiscale finite element method for elliptic problems in composite materials and porous media. J. Comput. Phys. **134**, 169–189 (1997)
Jenny, P., Lee, S.H., Tchelepi, H.A.: Adaptive multiscale finite-volume method for multiphase flow and transport in porous media. Multiscale Model. Simul. **3**(1), 50–64 (2005)
Karimi-Fard, M., Firoozabadi, A., et al.: Numerical simulation of water injection in 2d fractured media using discrete-fracture model. In: SPE Annual Technical Conference and Exhibition. Society of Petroleum Engineers (2001)
Karimi-Fard, M., Durlofsky, L.J ., Aziz, K., et al.: An efficient discrete fracture model applicable for general purpose reservoir simulators. In: SPE Reservoir Simulation Symposium. Society of Petroleum Engineers (2003)
Lee, S.H., Lough, M.F., Jensen, C.L.: Hierarchical modeling of flow in naturally fractured formations with multiple length scales. Water Resour. Res. **37**(3), 443–455 (2001)
Li, L., Lee, S.H., et al.: Efficient field-scale simulation for black oil in a naturally fractured reservoir via discrete fracture networks and homogenized media. In: International Oil & Gas Conference and Exhibition in China. Society of Petroleum Engineers (2006)
Logg, A.: Efficient representation of computational meshes. Int. J. Comput. Sci. Eng. **4**(4), 283–295 (2009)
Logg, A., Mardal, K.-A., Wells, G.: Automated Solution of Differential Equations by the Finite Element Method: The FEniCS Book, vol. 84. Springer, Berlin (2012)
Lunati, I., Jenny, P.: Multiscale finite-volume method for compressible multiphase flow in porous media. J. Comput. Phys. **216**(2), 616–636 (2006)
Martin, V., Jaffré, J., Roberts, J.E.: Modeling fractures and barriers as interfaces for flow in porous media. SIAM J. Sci. Comput. **26**(5), 1667–1691 (2005)
Mehmani, Y., Tchelepi, H.A.: Multiscale formulation of two-phase flow at the pore scale. J. Comput. Phys. **389**, 164–188 (2019)
Praditia, T., Helmig, R., Hajibeygi, H.: Multiscale formulation for coupled flow-heat equations arising from single-phase flow in fractured geothermal reservoirs. Comput. Geosci. **22**(5), 1305–1322 (2018)
Schwenck, N., Flemisch, B., Helmig, R., Wohlmuth, B.I.: Dimensionally reduced flow models in fractured porous media: crossings and boundaries. Comput. Geosci. **19**(6), 1219–1230 (2015)
Tene, M., Al Kobaisi, M.S., Hajibeygi, H.: Multiscale projection-based embedded discrete fracture modeling approach (f-ams-pedfm). In: ECMOR XV-15th European Conference on the Mathematics of Oil Recovery (2016a)
Ţene, M., Kobaisi, M.S.A., Hajibeygi, H.: Algebraic multiscale method for flow in heterogeneous porous media with embedded discrete fractures (f-ams). J. Comput. Phys. **321**, 819–845 (2016b)
Ţene, M., Bosma, S.B.M., Al Kobaisi, M.S., Hajibeygi, H.: Projection-based embedded discrete fracture model (pEDFM). Adv. Water Resour. **105**, 205–216 (2017)
Warren, J.E., Root, P.J., et al.: The behavior of naturally fractured reservoirs. Soc. Pet. Eng. J. **3**(03), 245–255 (1963)
Weinan, E., Engquist, B., Li, X., Ren, W., Vanden-Eijnden, E.: Heterogeneous multiscale methods: a review. Commun. Comput. Phys. **2**(3), 367–450 (2007)

Affiliations

Maria Vasilyeva[1,2] · Eric T. Chung[3] · Wing Tat Leung[4] · Valentin Alekseev[5]

✉ Maria Vasilyeva
vasilyevadotmdotv@gmail.com

Eric T. Chung
tschung@math.cuhk.edu.hk

1 Institute for Scientific Computation, Texas A&M University, College Station, TX 77843-3368, USA

2 Department of Computational Technologies, North-Eastern Federal University, Yakutsk, Republic of Sakha (Yakutia), Russia 677980

3 Department of Mathematics, The Chinese University of Hong Kong (CUHK), Shatin, Hong Kong SAR

4 Institute of Computational Engineering and Sciences, University of Texas at Austin, Austin, TX, USA

5 Multiscale model reduction laboratory, North-Eastern Federal University, Yakutsk, Republic of Sakha (Yakutia), Russia 677980